

# Signatures of Wannier-Stark and surface states in electron tunneling and related phenomena: Electron transmission through a tilted band

Alexander Onipko

*Department of Physics, Uppsala University, Box 530, S-751 21 Uppsala, Sweden and  
Department of Physics, IFM, Linköping University, S-581 83 Linköping, Sweden\**

Lyuba Malysheva

*Bogolyubov Institute for Theoretical Physics, Kiev, 03143, Ukraine*

(Received 29 April 2001; revised manuscript received 2 July 2001; published 29 October 2001)

As predicted by Wannier in 1960, band states quantization in a constant electric field  $E_n = \text{const} \pm n\mathcal{E}$ , where  $n=0,1,2, \dots$ , and  $\mathcal{E}$  is proportional to the strength of electric field [this kind of spectrum is commonly referred as the Wannier-Stark ladder (WSL)], implies that the probability of tunneling through a tilted band should have  $\mathcal{E}$  spaced peaks, at least, under the weak coupling of the band states to the source and drain electrodes. It has been discovered however [Phys. Rev. B **63**, 235 410 (2001)] that in finite-width crystals, the appearance of the canonical WSL is preceded by WSL's with other level spacing, namely,  $\mathcal{E}_{m'/m}/(1-2m'/m)$ , where  $m$  and  $m' < m/2$  are positive integers determined by the applied voltage. In the current article, the WSL's (including field-induced surface states) are discussed in the context of the electron quantum transport. On the basis of the tight-binding formalism and Green function technique we have developed a nonperturbative description of tunneling through a spatially finite tilted band. In this case, a resonance-type structure of the transmission spectrum of tunneling through a tilted band and its exponential dependence on the electric field strength are expected from physical arguments supported by earlier related studies. We have derived an explicit expression of the tunneling probability as a function of the energy of the tunneling electron, electric field strength and applied voltage. This exhibits some features of the tunneling process in the presence of the electric field, which have been missed in previous studies. The experimental implications of the results obtained are also outlined.

DOI: 10.1103/PhysRevB.64.195131

PACS number(s): 73.21.-b, 73.61.-r, 73.90.+f

## I. INTRODUCTION

In 1960 Wannier introduced the concept of the Wannier-Stark ladder (WSL), associated with the spectrum of electron band states in a constant electric field.<sup>1</sup> This gave rise to a vast number of publications aimed at developing an in-depth understanding of the electric field effects in solids. In the 1990's this activity resulted in several reports on the experimental observation of the Wannier-Stark (WS) effect, Bloch oscillations, and related coherent phenomena.<sup>2-4</sup> It also stimulated the appearance of new ideas such as, e.g., dynamic localization<sup>5</sup> and quasienergy band collapse in time-dependent electric fields.<sup>6-8</sup> The invention of optically driven lattices has uncovered new possibilities for studying quantum field effects.<sup>9-14</sup>

In its canonical form, the WSL represents a spectrum of evenly spaced electronic levels  $E_n = \text{const} \pm n\mathcal{E}$ , where  $n=0,1,2, \dots$ , and  $\mathcal{E}$  (the level spacing proportional to the strength of the electric field) is equal to the Planck constant times Bloch oscillation frequency. In the tight-binding formalism, this kind of spectrum is readily expected,<sup>15</sup> if the constant shift  $\mathcal{E}$  of the electron on-site (atomic) energy along the electric field is comparable to the width  $E_{\text{bw}}$  of the parent zero-field band of Bloch electron states. Such an extreme case of the WSL is of little, if any, physical interest though it is easy to think about. In most cases the perturbed band state spectrum emerges as a result of the delicate interplay of the electric field and interatomic interaction effects. Treating the

field parameter as small or large is equally inappropriate for their description.

In the early 1970's it was realized that the tight-binding model presents a unique opportunity to investigate the field effects in solids on a rigorous basis of the exact formal solution of the Schrödinger equation.<sup>16-19</sup> The corresponding Green function problem can also be solved without any restriction on the field parameter.<sup>20-22</sup> Though a number of important results have been obtained in this way,<sup>16-23</sup> the fundamental changes of the band spectrum of finite-thickness crystals in a constant electric field have not been elucidated completely.

In our recent work<sup>24</sup> which henceforth will be quoted as paper I, the full spectrum of a single tilted band has been classified in terms of a band of the bulk states affected by the field merging into two (lower and upper) bands of field-induced surface states. The former is termed the *extended states (es)* band, if the total electrostatic energy of the applied voltage  $eV$  is smaller than the zero-field band width  $E_{\text{bw}}$ . At higher voltages  $eV > E_{\text{bw}}$ , the term Wannier-Stark (WS) band seems to be appropriate. The *es* band width decreases with the increase of  $eV$  and shrinks to zero at  $eV = E_{\text{bw}}$ . Under certain voltages, the *es* levels form WSL's with the noncanonical level spacing  $q\mathcal{E}$ , where  $q (>1)$  is controlled by  $eV$  and can be an integer as well as a fractional number. The WS band, which opens at  $eV = E_{\text{bw}}$ , increases its width proportionally to  $eV$ . The finite-thickness corrections to the WSL levels in infinite crystals are exponentially

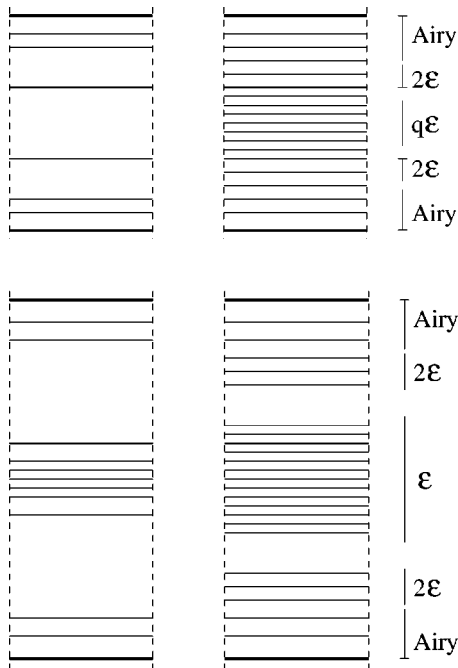


FIG. 1. The WSL as it appears from the infinite and semi-infinite crystal models (to the left) and its development (Ref. 24) (to the right); in the upper part  $eV=0.5E_{bw}$ , in the lower part  $eV=2.5E_{bw}$ ; Airy=Airy-type spectrum. Vertical dashed lines mark the crystal area; thick, thinner and thin horizontal lines indicate the band edges, subdivision of the band into  $s$  and  $e$  or WS band, and one-electron levels, respectively; blank spaces correspond to the energy intervals, where the spectrum does not have a simple explicit expression. To include surface states, the WSL concept is understood as a one-electron band spectrum determined by the only field parameter  $\mathcal{E}$ .

small but not zero. A fundamental difference between the  $e$ - and WS-band states is that the former is extended from the one side of the crystal to the opposite one, while the latter is separated from both crystal sides by the potential barriers of a triangular shape. (In an infinite crystal, these barriers are of infinite width).

As distinct from the WS states, the field-induced surface states are only separated from the other side of the crystal by a triangular barrier. They form what has been called the band of surface localized states ( $s$  bands) in the lower and upper parts (with respect to the bulk-state band) of the spectrum. It has been shown that the WSL actually merges into the  $s$  bands so that the  $\mathcal{E}$  spacing is characteristic not only for the WS band but also for the neighboring regions of the  $s$  bands. Away from the WS band, the level spacing increases. In the middle of the  $s$  bands, the electron levels are quantized with doubled Wannier quantum  $2\mathcal{E}$  while closer to the spectrum edges, the  $s$  level quantization behaves in a similar way to the zeroes of the Airy function.

These and other results have been derived in paper I from the above mentioned exact solution for the tight-binding model with a linear dependence of site energies on the field. Our findings regarding the band spectrum structure of finite-width crystals influenced by the electric field are schematically illustrated in Fig. 1. Those of the results which are of

special interest for present consideration will be discussed below in more detail.

The Wannier-Stark effect is intimately interconnected with two other fundamental electric field effects in solids: Zener tunneling<sup>25</sup> and Franz-Keldysh absorption.<sup>26</sup> Both of them involve at least two bands affected by the electric field. Long ago an exponential dependence on the field parameter was shown to be a distinctive feature of both effects. A widely used expression of the exponential factor in the Zener tunneling probability has been given by McAfee *et al.*<sup>27</sup> and Keldysh,<sup>28</sup> and rederived by Kane.<sup>29</sup> A similar factor in the interband transition probability has been deduced by Keldysh.<sup>26</sup> All the derivations cited imply a small value of  $eV$  in comparison with the band gap and band widths of the zones in question that is not the case in most experiments. In this sense the original works<sup>26-29</sup> and subsequent publications,<sup>30-33</sup> treated the electrostatic energy  $eV$  as a small perturbation.<sup>34</sup>

In the nonperturbational approach, this energy, the band gap and band widths have to be considered on an equal footing. However, the use of basis sets for an infinite crystal and particularly the basis wave functions subjected to periodic boundary conditions (which are in a natural conflict with the electric field effect breaking the system periodicity) complicates if not precludes the development of a consistent non-perturbative technique. With the use of such basis sets, a good deal of mastery and unique physical intuition are required to obtain correct results regarding electric field effects. These were certainly present in the classical works cited. In their later developments, which are too vast to be covered here, the functional form of the exponential factor has never been questioned. This makes it all the more important to go beyond the Keldysh and Kane approximations without the loss of readability of classical analytical results.

An approach based on the exact Green function of the tight-binding model, which is the method we use in paper I and the present work, is free from the above mentioned difficulties. An obvious advantage is that once the model is defined, neither of characteristic parameters is treated as a perturbation. Another advantage is that each principal step of the analytical analysis can be unambiguously controlled by exact computer calculations. So instead of believing or disbelieving the derived results, one may just compare them with what a computer says. Now and then such a check has been illustrated in paper I, and we continue to do so in present consideration.

A consistent description of Zener tunneling and Franz-Keldysh absorption is a hard task even for reasonably simplified models. Both effects may be thought to include tunneling through a tilted band (more precisely a bent band) as a certain stage of the process. Here therefore we concentrate on a detailed analytical description of this stage which is a single-band problem. Its solution is also valuable in itself. The tunneling through a single tilted band occurs when, for instance, electrons are transmitted through a superlattice and both the electron tunneling energy and the electrostatic energy of the applied voltage do not much exceed the width of the lowest miniband. This is the most obvious example but not the only one, where the present model is straightforward.

wardly applicable on a full scale.

The main contribution of this work is seen in obtaining an explicit expression of the tunneling probability through a spatially finite tilted band. It reveals the resonance structure of the transmission spectrum and its dependence on the characteristic parameters of the system. To a certain extent, details of this dependence are model dependent. Most of the conclusions, however, are of a wide significance. In particular, the resonance structure is shown to have distinctive regularities within the *es*-, *s/s*-, and WS-band energy intervals. Except in the case of the *es* band, the tunneling probability is governed by an exponential factor. The functional form of the exponent does not depend on how an electron happens to go in and come out of the tunneling region. This has enabled us to find the exponential factors which describe tunneling through the *s/s* and WS bands, by using a simple but somewhat *ad hoc* procedure.<sup>35</sup> One purpose of this work is also to give a rigorous proof of these factors. But above all the present analysis of tunneling through a single tilted band opens the door to a nonperturbative analytical description of more complex tunneling phenomena. The Zener tunneling will be addressed next.

This presentation is organized as follows. In Secs. II and III, the model system of source-(tunneling-region) drain and basic equations for its description are briefly introduced. Equation (3) for the transmission coefficient and a set of Green functions in Eqs. (5) and (6) are most important for the rest of discussion. Each of the two has a long story of its own and the both of them belong to the established results in the respective field. Nevertheless a mass of different approaches, methods, physical contexts, notations, etc. may make it difficult to see the links between our starting equations, and the initial Schrödinger problem with the scattering boundary conditions. It seems worth mentioning therefore that our two earlier works<sup>22,36</sup> contain all the major steps of the derivation of Eq. (3), and Eqs. (5) and (6). The model exact expression of the transmission coefficient [which is given in Eq. (3) and also used to be called the tunneling probability] is examined for the energy regions of bulk electron states at low voltages (in Sec. IV), surface localized states (in Sec. V), and bulk electron states at high voltages (in Sec. VI). Section VII represents the case of tunneling outside the band spectrum, and Sec. VIII outlines our main findings and the possibilities of their experimental verification.

## II. MODEL

We have chosen to discuss the electric field effects on tunneling through a spatially finite and energetically restricted band of electron states in the context of ballistic charge transport in superlattices, where the lowest miniband can be artificially made separate. However, our model is equally applicable to any thin dielectric monolayer whose electron spectrum (in the direction of the electric field) contains a well defined unfilled band which mixes weakly with the other bands in the actual range of the applied voltage.

The profile of an  $\mathcal{N}$ -well superlattice model potential is shown by a dashed line in Fig. 2. Due to the electron con-

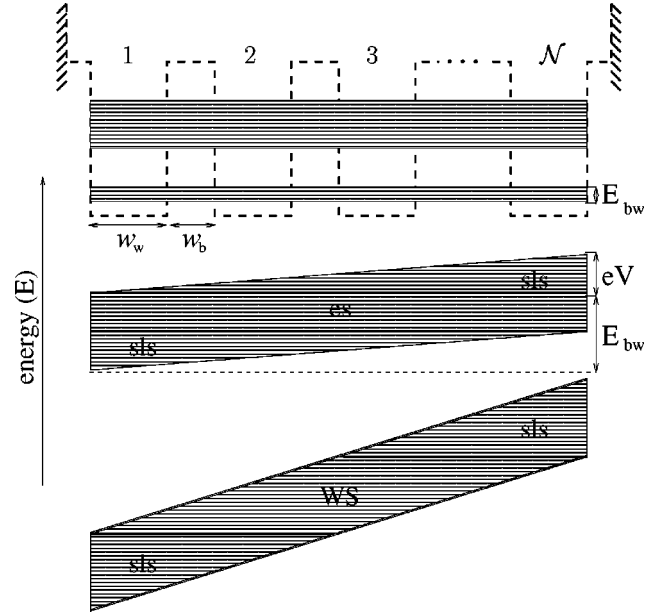


FIG. 2. Upper part: potential energy profile of an  $\mathcal{N}$ -well superlattice and its two lowest minibands appearing due to the inter-well tunneling. For a superlattice  $(\text{Al}_x\text{Ga}_{1-x}\text{AsAl}_x^*\text{Ga}_{1-x}^*\text{As})_{\mathcal{N}}$  with the well width  $w_w=100 \text{ \AA}$ , barrier width  $w_b=40 \text{ \AA}$ , barrier height  $=0.3 \text{ eV}$ , and electron effective mass  $=0.066m_e$ , the lowest miniband width (for  $\mathcal{N} \gg 1$ )  $E_{bw}=3.7 \text{ meV}$ , which is 24 times smaller than the band gap (Ref. 7). Lower part: The lowest miniband tilted by the applied potential  $eV$ , which is smaller (up) and larger (down) than  $E_{bw}$ .

finement in a well, the well spectrum is quantized. Due to tunneling between neighboring wells, the discrete (in its lower part) spectrum of an isolated well splits into minibands of allowed electron energies that are separated by energy gaps, which do not contain electron states. Since the height and width of the barriers can be freely engineered within a wide range, it is definitely possible to have the lowest miniband separated from the others by an energy interval much exceeding its band width  $E_{bw}$ . An example of this kind is represented in Fig. 2.

Under a restriction that the electrostatic potential drop across the superlattice does not much exceed the magnitude of  $E_{bw}$ , the description of the electron transport along the superlattice can be started from the Hamiltonian matrix for a single band

$$H_{nn'} = \mathcal{E}[n - (\mathcal{N} + 1)/2] \delta_{n,n'} + \delta_{|n-n'|,1}, \quad (1)$$

where (see Fig. 2) indices  $n, n' = \overline{1, \mathcal{N}}$  number the wells in the superlattice;  $\mathcal{E} = eFa/\beta$ ;  $e$ ,  $F$ , and  $a$  are, respectively, the electron charge absolute value, electric field strength, and superlattice periodicity  $a = w_w + w_b$ ; the energy of electron resonance transfer between neighboring wells  $\beta$  serves as an energy unit; the zero-field energy of the lowest level in the noninteracting wells (the electron on-site energy) is set equal to zero.

The eigenvalues of the Hamiltonian matrix (1) lie within the (dimensionless) energy interval which is equal to  $E_{bw}$

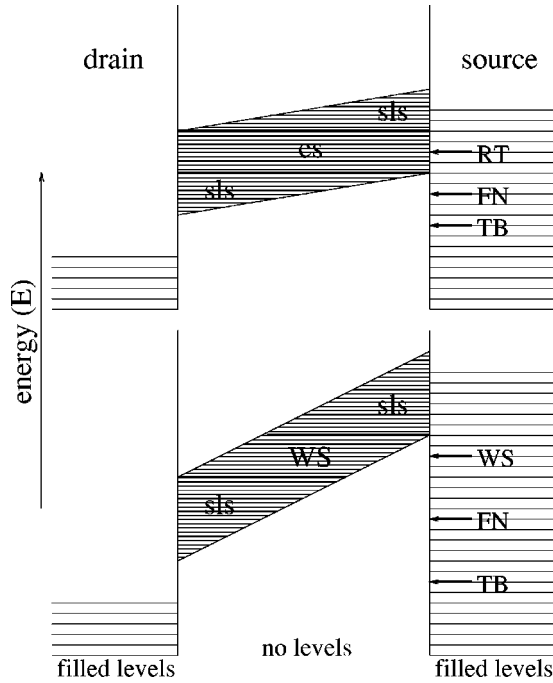


FIG. 3. Energy diagrams of lead-superlattice-lead heterostructure. The electron spectrum of the superlattice is modeled by a single tilted band. At low voltages  $eV < E_{\text{bw}}$  (upper diagram) the electron energy can be tuned to  $es$ -band (resonance tunneling, RT arrow),  $sfs$  band (Fowler-Nordheim type tunneling, FN arrow), or it can be out of the tilted band spectrum (through trapezoid barrier tunneling, TB arrow). The high voltage case is distinct only by that tunneling through the mid-part of the tilted band is assisted by Wannier-Stark states (WS arrow).

$+eV$ , with  $eV = \mathcal{E}(\mathcal{N} - 1)$ , and  $E_{\text{bw}} = 4$  in units of  $\beta$ . Excluding classically inaccessible regions in the  $n$ - $E$  “coordinates,” one obtains a tilted band of electron states. Such a band is shown in Fig. 2 for two voltages  $eV < E_{\text{bw}}$  and  $eV > E_{\text{bw}}$ . The sloped lines on the band diagrams indicate the  $n$ - $E$  (unshaded) regions, where the probability of finding an electron with the given energy in a well  $n$  ( $= 1, 2, \dots, \mathcal{N}$ ) is proportional to the tailing part of the corresponding squared eigenfunction of  $H_{nn'}$ . As seen from the figure, if the applied potential is smaller than the miniband width in the zero field,  $eV < E_{\text{bw}}$ , the band spectrum can be divided into one  $es$  band and two  $sfs$  bands; at higher voltages  $eV > E_{\text{bw}}$ , the  $es$  band is replaced by a WS band.

Let us assume that from its opposite boundary layers, the superlattice is contacted homogeneously to ideal semi-infinite drain and source electrodes and that the interaction between its first ( $\mathcal{N}$ th) well and the drain (source) lead can be described by a single parameter  $\mathcal{V}$ . The latter means the electron resonance transfer energy from an atom on the metal surface to the first ( $\mathcal{N}$ th) terminal well of the superlattice. Furthermore according to the model, the electrostatic potential energy inside the leads is constant (though different) and drops from the source to drain by the magnitude of  $eV$ , entirely in the region occupied by the superlattice, see energy diagrams in Fig. 3. Also suppose that the spatial variables of the Hamiltonian of the system drain-superlattice source are

separable and that the field is directed along one of the principal axes. Then, the electron energy  $E$  can be broken into a sum of two nonmixing components which correspond to the energy of electron motion parallel ( $E_{\parallel}$ ) and perpendicular ( $E_{\perp}$ ) to the electric field and the superlattice growth direction. In such a system, an electron wave having the energy  $E$  and propagating freely in the source electrode towards the drain electrode, will be transmitted through the superlattice with the probability  $T(E, E_{\perp})$ . For the model outlined above, finding the transmission probability is a one-dimensional problem.

### III. BASIC EQUATIONS

Due to the Landauer-Büttiker theory<sup>37–39</sup> and earlier works,<sup>40</sup> the transmission probability is directly related to the current-voltage relation. Several established methods can be used to calculate  $T(E, E_{\perp})$ , see, e.g., Ref. 41. The Green function technique is known to be particularly useful for the development of efficient computational schemes and analytical analysis.

Probably it was Caroli *et al.*<sup>42</sup> who first proposed describing tunnel current in metal-insulator-metal heterostructures in the Green function language. Later on their treatment has been reformulated in a number of physical contexts to examine, in particular, the quantum conductance of molecular wires.<sup>36,43–45</sup> Although the methodology of the electron transport theory is well developed, it seems to be instrumental in outlining the derivation of the transmission coefficient which then serves as a starting point of the original analysis.

In the framework of the Green function formalism,  $T(E, E_{\perp})$  is conveniently expressible in terms of the Green functions referring the noninteracting source and drain leads and the scattering region, which here is the superlattice. For the model specified in the preceding section, the transmission probability can be represented as

$$T(E, E_{\perp}) = 4 \text{Im}(\hat{\Sigma}^D)_{11} \text{Im}(\hat{\Sigma}^S)_{\mathcal{N}\mathcal{N}} \left| \left( \frac{1}{E\hat{I} - \hat{H} - \hat{\Sigma}^D - \hat{\Sigma}^S} \right)_{1,\mathcal{N}} \right|^2, \quad (2)$$

where the matrix of Hamiltonian operator  $\hat{H}$  is given in Eq. (1), the self-energy operator is defined as  $(\hat{\Sigma}^{D(S)})_{nn'} = \delta_{n,n'} \delta_{n,1(\mathcal{N})} (\mathcal{V}^2/\beta) G^{D(S)}(E, E_{\perp}, eV)$ , and  $G^{D(S)}(E, E_{\perp}, eV)$  is the surface diagonal matrix element of the drain (source) lead. Notice that Eq. (2) is nothing but a particular case of the exact general expression which relates the transmission probability to the Green function of the open system.<sup>41</sup> Details of the derivation of Eq. (2) can be found in Ref. 36.

The real and imaginary parts of self-energy determine the shift and broadening of superlattice levels as a result of their interaction with the metal pads. In general, they are energy dependent. However the miniband width and the range of changes of  $eV$  are far much smaller than the Fermi energy  $E_F$  of the contacting leads. On the other hand, for small

variations of energy and applied voltage, the local surface density of states  $\pi^{-1} \text{Im} G^{D(S)}(E, E_{\perp}, eV)$  differs only negligibly from its value at the Fermi energy  $\pi^{-1} \text{Im} G^{D(S)}(E_F)$ . Moreover, the imaginary part is normally much larger than

the real part of the same diagonal matrix element. It is therefore justifiable to set  $(\hat{\Sigma}^D)_{11} = (\hat{\Sigma}^S)_{\mathcal{N}\mathcal{N}} = i(\mathcal{V}^2/\beta) \text{Im} G^D(E_F) = i(\mathcal{V}^2/\beta) \text{Im} G^S(E_F) \equiv iA$ . With these simplifications, Eq. (2) takes the form

$$T(E) = \frac{4A^2 G_{1,\mathcal{N}}^2(E)}{[1 + A^2 G_{\Delta}(E)]^2 + A^2 [G_{11}(E) - G_{\mathcal{N}\mathcal{N}}(E)]^2 + 4A^2 G_{1,\mathcal{N}}^2(E)}, \quad (3)$$

where  $G_{\Delta}(E) = G_{11}(E)G_{\mathcal{N}\mathcal{N}}(E) - G_{1,\mathcal{N}}^2(E)$  and the (superlattice) Green function obeys the equation

$$\sum_{n''=1}^{\mathcal{N}} (E \delta_{nn''} - H_{nn''}) G_{n''n'}(E) = \delta_{nn'}. \quad (4)$$

Hence the matrix elements  $G_{nn'}(E)$  are the only quantities in Eq. (3) which have to be found. They depend solely on  $E_{\parallel}$  and so does the transmission coefficient. Therefore in Eqs. (3), (4) and henceforth the subscript  $\parallel$ , as well as the indication of the Green function and the transmission coefficient dependence on the field and width of the tunneling region, are omitted for brevity.

As mentioned in the introduction, Eq. (4) has an exact analytical solution. Its derivation is very similar to the exact formal solution of the corresponding Schrödinger problem  $\hat{H}\Psi = E\Psi$ , found by Stay and Gusman<sup>17</sup> for the open-ends boundary conditions which are used here, and by Saitoh<sup>18</sup> for the periodic boundary conditions. The solution involves rather cumbersome algebra and can be represented in several equivalent forms. For the conventions regarding the site numbering and energy reference point accepted in Eq. (1), expressions of  $G_{11}(E) = -G_{\mathcal{N}\mathcal{N}}(-E)$  and  $G_{1,\mathcal{N}}(E)$  are given by<sup>22</sup>

$$D_{\mathcal{N}}(E, \mathcal{E}) G_{11}(E) = J_{\mu+(\mathcal{N}-1)/2}(z) Y_{\mu-(\mathcal{N}+1)/2}(z) - Y_{\mu+(\mathcal{N}-1)/2}(z) J_{\mu-(\mathcal{N}+1)/2}(z), \quad (5)$$

$$D_{\mathcal{N}}(E, \mathcal{E}) = J_{\mu+(\mathcal{N}+1)/2}(z) Y_{\mu-(\mathcal{N}+1)/2}(z) - Y_{\mu+(\mathcal{N}+1)/2}(z) J_{\mu-(\mathcal{N}+1)/2}(z), \quad (6)$$

and  $D_{\mathcal{N}}(E, \mathcal{E}) G_{1,\mathcal{N}}(E) = \mathcal{E}/\pi$ , where  $\mu \equiv E/\mathcal{E}$ ,  $z \equiv 2/\mathcal{E}$ , and  $J_{\mu}(z)$  and  $Y_{\mu}(z)$  are the Bessel functions of the first and second kind, respectively.

Before going into a detailed discussion of  $T(E)$  dependence on energy, field strength, and superlattice length, some relevant remarks might be useful. As is mentioned above the  $n$ - $E$  areas of different shape, which are classically accessible for electrons (shaded in Figs. 2 and 3) are distinct in their physical properties. Depending on whether the electrostatic energy is smaller or larger than the zero-field band width, we have either a rectangular or parallelogram in between two triangles. The voltages restricted by the conditions  $eV < E_{\text{bw}}$  and  $eV > E_{\text{bw}}$  will be referred as low and high voltages, respectively. The qualitative difference between the

two cases stems from the fact that the electron states extended over the entire superlattice can exist at low voltages, but not at high voltages, when the  $es$  band is closed and the WS band opens instead.<sup>24</sup>

Contrary to extended states, which “connect” the source and drain electrodes, the electron states located within either of the two triangular areas are separated from the other side of the superlattice by a triangular barrier, see Fig. 3. This implies that the eigenstates of Hamiltonian (1), whose energies are within the shaded triangles, have the amplitude which decays exponentially with  $n$  (lower triangle) or  $\mathcal{N} - n$  (upper triangle), if the corresponding pair of coordinates  $n$ - $E$  or  $(\mathcal{N} - n)$ - $E$  is outside the shaded area. This justifies the use of the term “surface localized states.” (The field induced  $s$ ls do exist, if  $\mathcal{E} \geq 12.2/\mathcal{N}^3$ .<sup>24</sup>) Similarly two triangular barriers from both sides of the WS band make the WS states localized. These states decay exponentially away from the shaded parallelogram.

It is thus obvious that depending on the applied voltage and energy of electrons being transmitted through the superlattice, the electron flux may encounter no barriers at all, one triangular barrier, two triangular barriers, or a trapezoid barrier, as exemplified by arrows labeled in Fig. 3 by RT, FN, WS, and TB. Correspondingly, we distinguish between physically different cases of  $es$ -assisted or resonance tunneling (arrow RT),  $s$ ls-assisted or Fowler-Nordheim-type tunneling (arrow FN), WS states assisted tunneling (arrow WS), and through trapezoid barrier tunneling (arrow TB).

Tunneling through trapezoid and triangular barriers has been extensively studied in the WKB approximation.<sup>46</sup> Such an approach is inapplicable for the description of the present discrete finite band model. In particular it fails to reproduce the resonance structure of  $T(E)$ , which might be expected for the  $s$ ls-assisted tunneling, that is tunneling through a triangular well. Concerning the resonance tunneling transmission, the energy and length dependence of  $T(E)$  in zero field  $\mathcal{E} = 0$  has been examined previously.<sup>43</sup> However as is shown in paper I, the presence of an electric field gives rise to the noncanonical WSL which should be specifically reflected in the transmission spectrum. The expected resonance structure of  $s$ ls- and WS-assisted tunneling probability is of the same nature as the oscillations predicted for the Zener tunneling probability<sup>30,47</sup> and absorption coefficient.<sup>31–33,48</sup> However, no conclusive analytical results have been obtained so far for the tunneling through a finite tilted band. In the following sections, the transmission spectrum will be examined in the

RT, FN, WS, and TB energy intervals, where accurate explicit expressions of  $T(E)$  can be derived from the model exact equations (3), (5), and (6).

#### IV. TUNNELING ASSISTED BY EXTENDED STATES

The noncanonical WSL's which represent energy levels of extended states lying in the middle of the band spectrum, have been introduced and studied in paper I. As already emphasized, this kind of level quantization is characteristic only for the spectrum midpart and appears at the voltages  $eV_{m'/m} = (\mathcal{N}-1)\mathcal{E}_{m'/m} < E_{\text{bw}}$  satisfying the condition

$$(\mathcal{N}-1)\mathcal{E}_{m'/m} = 4 \cos\left(\pi \frac{m'}{m}\right), \quad (7)$$

where  $m$  and  $m' < m/2$  are positive integers,  $m = 3, 4, \dots$ . For these values of field parameter  $\mathcal{E}_{m'/m}$ , the eigenenergies of Hamiltonian (1) form a WSL

$$E_l = \left\{ \begin{array}{l} l \\ l+1/2 \end{array} \right\} \frac{1}{1-2m'/m} \mathcal{E}_{m'/m}, \quad (8)$$

with the upper (lower) factor standing for an odd  $\mathcal{N} = 2N + 1$  (even  $\mathcal{N} = 2N$ ) number of wells in the superlattice.

It is seen that the level spacing in Eq. (8) is equal to  $\mathcal{E}$  times a numerical factor  $q = 1/(1-2m'/m)$  which is larger than unity and takes either an integer or fractional value. Thus unlike the canonical WSL, the equidistant spectrum (8) holds true only for *certain* values of the field parameter. Any of the noncanonical WSLs can be obtained only at a unique voltage. For instance the WSL with triple- $\mathcal{E}$  level spacing should appear when the electrostatic energy is exactly equal to  $E_{\text{bw}}/2$  if  $\mathcal{N}$  is odd, or to  $E_{\text{bw}}/2 - \mathcal{E}$ , if  $\mathcal{N}$  is even.

From the experimental point of view, the spectrum of the type (8)  $E_l = lq\mathcal{E}$  is clearly distinguishable from the WS spectrum  $E_n = n\mathcal{E}$ , especially if  $q = 2, 3, \dots$  or  $q = 1$

+  $2m'/(m-2m')$  with a not too small second summand. It should be also noticed that Eq. (8) is accurate only for sufficiently large values of  $\mathcal{N}$ . For some voltages the correspondence between the approximate WSL energies and exact eigenvalues [solutions to  $\mathcal{D}_{\mathcal{N}}(E, \mathcal{E}) = 0$ ] can be seen in Fig. 4, where the former and the latter are indicated by circles and stars, respectively. In our example,  $\mathcal{N} = 101$ ; the increase or decrease of  $\mathcal{N}$  will improve or worsen the accuracy of Eq. (8).

To expose noncanonical WSL's in the transmission spectrum, we obtain an approximation of the Green function matrix elements at the energies  $E_n = n\mathcal{E}$  with  $n$  equal to a positive integer subjected to the condition  $n \ll \mathcal{N}$ . Using these restrictions in Eqs. (5) and (6), and performing algebra which is quite in the spirit of the derivation of Eqs. (7) and (8),<sup>24</sup> we get

$$G_{11}(E_n) \approx \frac{\sin[(2n-1)\chi]}{\sin(2n\chi)}, \quad (9a)$$

$$G_{\mathcal{N}\mathcal{N}}(E_n) \approx -\frac{\sin[(2n+1)\chi]}{\sin(2n\chi)}, \quad (9b)$$

$$G_{1\mathcal{N}}(E_n) \approx (-1)^{N+n+1} \frac{\sin \chi}{\sin(2n\chi)}, \quad (9c)$$

where  $\chi = \arccos(\mathcal{E}N/2)$ . Unlike the exact expressions for the Green function matrix elements, Eqs. (9a), (9b), and (9c) make sense only for large values of  $\mathcal{N}$  (set to be odd), and only for the indicated energies. The substitution of the above expressions in Eq. (3) yields

$$T(E = n\mathcal{E}) \approx \frac{4A^2 \sin^2 \chi}{4A^2 \sin^2 \chi + \sin^2(2n\chi)[1 + 2 \cos(2\chi)A^2 + A^4]} \quad (10a)$$

or, equivalently,

$$T(n\mathcal{E}) \approx \frac{A^2(4 - \mathcal{E}^2 N^2)}{A^2(4 - \mathcal{E}^2 N^2) + \sin^2[2n \arccos(\mathcal{E}N/2)][(1 - A^2)^2 + A^2 \mathcal{E}^2 N^2]}. \quad (10b)$$

Note that Eq. (10a) is also valid for high voltages in which case  $\chi = \cosh^{-1}(\mathcal{E}N/2)$ , and  $\sin \chi$  and  $\cos \chi$  should be replaced by  $\sinh \chi$  and  $\cosh \chi$ , respectively.

According to Eq. (10b), if the applied potential satisfies Eq. (7), the transmission coefficient is equal to unity for  $E = n\mathcal{E}$  with  $n$  divisible by  $m$ , if  $m$  is odd, or by  $m/2$ , if it is even. This result makes it obvious that  $T(E)$  has a resonancelike structure which means that at a fixed voltage, the transmission spectrum as a function of energy has maxima. Alternatively at a fixed energy, it exhibits maxima as a function of the applied voltage. The noncanonical WSL's are thus exposed in the transmission spectrum (see Fig. 4) as almost equidistant peaks. The level spacing is in good agreement with formula (8). However, approximation (10) does not re-

produce the observed decrease of transmission peak maxima away from the spectrum center. As well seen in Fig. 4, such a decrease is a pronounced tendency of the exact dependence of the transmission probability on energy. It reflects a general trend of resonance tunneling phenomena implying that the total transmission is only possible in totally symmetric systems. In the given case, the system symmetry is broken by the applied potential. The increase of  $eV$  results in an increasing suppression of the transmission peaks close to the  $es$ -band edges. A similar effect of suppressing the electron transmission by the applied potential is known in conventional barrier-well-barrier heterostructures.<sup>49</sup>

Figure 4 also reveals a specific property of noncanonical WSL's that is in apparent seeming conflict with physical ar-

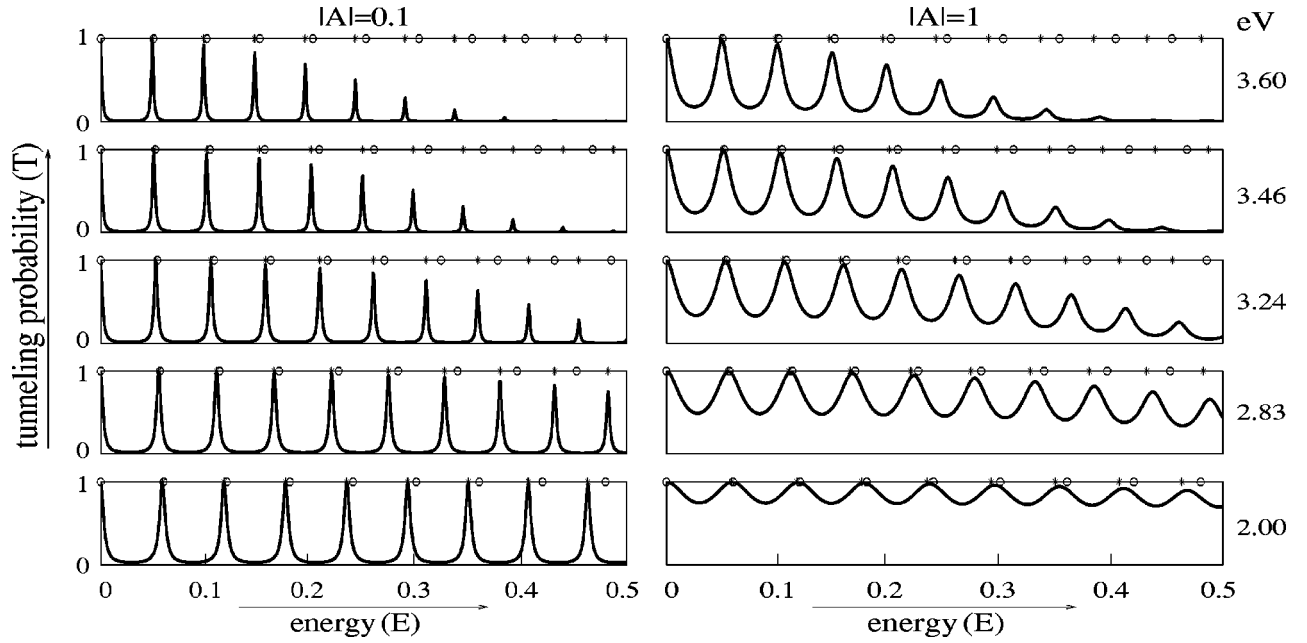


FIG. 4. Miniband transmission spectrum evolution under increasing voltage: from bottom to top  $eV=2.00, 2.83, 3.24, 3.46,$  and  $3.60$ ;  $\mathcal{N}=101$ . The exact level energies, i.e., solutions to  $D_{\mathcal{M}}(E, \mathcal{E})=0$ , are indicated by stars. WSLs with noncanonical level spacing  $3\mathcal{E}_{1/3}, 2\mathcal{E}_{1/4}, \frac{5}{3}\mathcal{E}_{1/5}, \frac{3}{2}\mathcal{E}_{1/6},$  and  $\frac{7}{5}\mathcal{E}_{1/7}$  are labeled by open circles.

guments. The comparison of the peak positions for ever larger potential (from bottom to top) shows that the peak spacing *decreases* with the *increase* of  $\mathcal{E}$ . This is a reflection of the predicted increase of the density of states in the mid-part of the spectrum in response to voltage increase within the range  $0 < eV < E_{\text{bw}}$ .<sup>24</sup> Such behavior makes the noncanonical WSL's even more easily distinguishable from those predicted by Wannier because for the latter, the level spacing and hence peak spacing increases with  $eV$ .

Finally for illustrative purposes Fig. 4 represents transmission spectra of the *es*-assisted tunneling for a smaller (to the right) and larger value of the effective superlattice-to-lead coupling  $|A|$ . With the increase of this parameter, the transmission peaks broaden which is a kind of behavior expected from other resonance tunneling structures.

## V. TUNNELING ASSISTED BY SURFACE LOCALIZED STATES

By using the standard approximations of Bessel functions with large arguments and small or large orders,<sup>50</sup> it can be shown that the exact expressions of  $G_{11}(E)$ ,  $G_{\mathcal{N}\mathcal{N}}(E)$ , and  $G_{1\mathcal{N}}(E)$  [see Eqs. (5) and (6)] are accurately reproduced

within the *s/s*-band energy interval  $|(E_{\text{bw}} - eV)/2| + \mathcal{E} < E < (E_{\text{bw}} + eV)/2 - \mathcal{E}$  by the following relations:

$$\left\{ \begin{array}{l} D_{\mathcal{M}}(E, \mathcal{E}) \\ D_{\mathcal{M}}(E, \mathcal{E}) G_{11}(E) \\ D_{\mathcal{M}}(E, \mathcal{E}) G_{\mathcal{N}\mathcal{N}}(E) \end{array} \right\} \approx \frac{\mathcal{E}/\pi}{\sqrt{\sin \xi \sinh \delta}} \exp\left(\frac{2}{\mathcal{E}} \Phi_{\delta}\right) \times \left\{ \begin{array}{l} \cos\left(\frac{2}{\mathcal{E}} \Phi_{\xi} - \frac{\pi}{4} + \xi\right) e^{\delta} \\ \cos\left(\frac{2}{\mathcal{E}} \Phi_{\xi} - \frac{\pi}{4} + \xi\right) \\ \cos\left(\frac{2}{\mathcal{E}} \Phi_{\xi} - \frac{\pi}{4}\right) e^{\delta} \end{array} \right\}, \quad (11)$$

where  $2 \cosh \delta = E + eV/2$ ,  $\Phi_{\delta} = \delta \cosh \delta - \sinh \delta$ ,  $2 \cos \xi = E - eV/2$  ( $0 \leq \xi \leq \pi$ ), and  $\Phi_{\xi} = \sin \xi - \xi \cos \xi$ . Note that the excluded  $\mathcal{E}$  intervals cannot contain more than one *s/s* level each.

Using the above expressions in Eq. (3), we get

$$T(E) = \frac{4A^2 \sinh \delta \sin \xi \exp(-2\delta)}{(1 + A^2 e^{-2\delta}) \left[ \cos^2\left(\frac{2}{\mathcal{E}} \Phi_{\xi} - \frac{\pi}{4} + \xi\right) + A^2 \cos^2\left(\frac{2}{\mathcal{E}} \Phi_{\xi} - \frac{\pi}{4}\right) \right]} \exp\left(-\frac{4}{\mathcal{E}} \Phi_{\delta}\right), \quad (12)$$

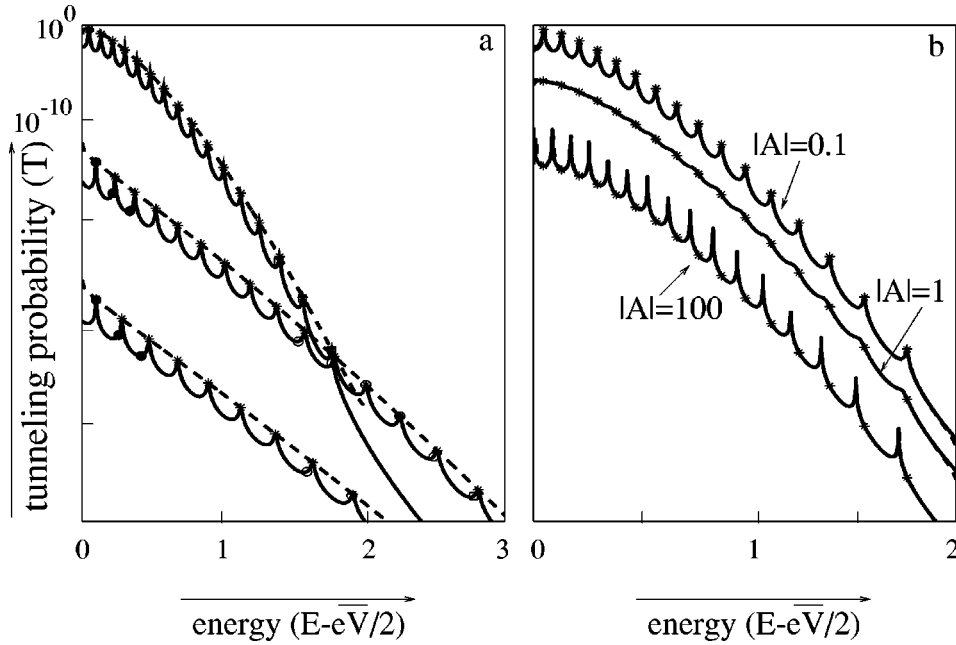


FIG. 5. Transmission spectrum of *s/s*-assisted tunneling through the lowest miniband of a 51-well superlattice. (a) The miniband is tilted by the electrostatic potential difference  $eV$  of (up to down)  $0.5E_{\text{bw}}$ ,  $1.5E_{\text{bw}}$ , and  $2E_{\text{bw}}$ ;  $|A|=0.1$  (weak coupling). Open and filled circles indicate  $\mathcal{E}$ - and  $2\mathcal{E}$ -spaced peaks; and those peaks, which follow the Airy spectrum  $2 + eV/2 - E_n = [3\pi(n - 1/4)\mathcal{E}/2]^{2/3} - \mathcal{E}$  (Ref. 24) are indicated by squares. Dashed envelopes represent Eq. (13) with  $E_n^{s/s}$  replaced by  $E$ . (b)  $T(E)$  is calculated from Eq. (3) (solid lines) and Eq. (12) (dashed line) for  $eV=0.5E_{\text{bw}}$  and  $|A|=0.1$  (weak coupling), 1 (intermediate coupling), and 100 (strong coupling). In both figures (a) and (b), stars indicate the values of  $T(E_n^{s/s})$ .

exhibiting a resonancelike structure modulated by a function  $\exp(-4\Phi_\delta/\mathcal{E})$  that decays exponentially with the increase of energy.

For the energies of the *s/s*-band levels  $E_n^{s/s}$ , given by solutions to equation  $\mathcal{D}_N(E, \mathcal{E}) \sim \cos(2\Phi_\delta/\mathcal{E} - \pi/4 + \xi) = 0$  within the energy interval  $[(E_{\text{bw}} - eV)/2, (E_{\text{bw}} + eV)/2]$ ,<sup>24</sup> expression (12) simplifies to

$$T(E_n^{s/s}, \mathcal{E}) = \frac{4 \sinh \delta_n \exp(-2\delta_n)}{\sin \xi_n [1 + A^2 \exp(-2\delta_n)]} \exp\left(-\frac{4}{\mathcal{E}} \Phi_\delta\right), \quad (13)$$

where  $\delta_n = \cosh^{-1}(E_n^{s/s}/2 + eV/4)$  and  $\xi_n = \arccos(E_n^{s/s}/2 - eV/4)$ . In the case of weak superlattice-to-lead coupling  $A^2 \ll 1$ , Eq. (13) determines local maxima of  $T(E)$ . Thus with the replacement  $E_n^{s/s} \rightarrow E$ , the right-hand side (RHS) of Eq. (13) gives a function that envelops the peaks of transmission spectrum in the region of *s/s*-assisted tunneling.

As seen in Fig. 5, except a small  $\mathcal{E}$  interval above the top of the *es* or WS band, an explicit analytical description of the *s/s*-assisted tunneling given by Eq. (12) is indistinguishable from exact calculations. This is a central result of the section. It might be worth emphasizing that the details of the resonance structure of  $T(E)$ , e.g., the width and intensity of the peaks, are model dependent. The factor  $\exp(-4\Phi_\delta/\mathcal{E})$  prescribes an exponential *decrease* with the increase of energy (counted from the spectrum center) and an exponential *increase* with the increase of electric field strength for the *s/s*-assisted tunneling probability. This is characteristic for the linear drop of the electrostatic potential within the scattering

region. It does not depend therefore on a particular model of the interface and connection to the leads. The reason for this is that the *s/s*-assisted tunneling is controlled by the exponential tailing of the *s/s* wave function in the classically forbidden region.

The exponential decay of the probability of tunneling through the *s/s* band can be evaluated from the ratio of the probabilities to find an electron with, say, the energy  $E_n^{s/s}$  in the first and last wells of the isolated superlattice. Such an approach, which is much more simple technically (since the leads and connection to them are not considered), gives a reasonable result even for the pre-exponential factor of the enveloping function<sup>35</sup>  $T(E_n^{s/s}, \mathcal{E}) = (\sinh \delta_n / \sin \xi_n) \times \exp(-2\delta_n) \exp(-4\Phi_\delta/\mathcal{E})$ , which differs from the correct expression (13) only by factor of 4.

To make Eqs. (12) and (13) easy readable, one can use an approximate expression

$$3\Phi_\delta \approx \begin{cases} (E - \overline{eV}/2)^{3/2}, & eV \leq E_{\text{bw}}, \\ (E + \overline{eV}/2)^{3/2}, & eV > E_{\text{bw}}, \end{cases} \quad (14)$$

where  $\overline{eV} = |eV - E_{\text{bw}}|$  is the excess of electrostatic potential energy over zero-field band width, and  $\overline{eV}/2$  means the top of the *es* band (WS band) for the low (high) voltages. The above approximation reproduces the exact dependence reasonably well up to  $\overline{eV}$  of the order of  $E_{\text{bw}}$ , see Fig. 6.

With the use of Eq. (14) in Eqs. (12) and (13), the exponential factor  $\exp(-4\Phi_\delta/\mathcal{E})$  in the latter equations can be replaced by  $\exp[-4(E - \overline{eV}/2)^{3/2}/(3\mathcal{E})]$  if  $eV < E_{\text{bw}}$ . A similar factor appears in the Fowler-Nordheim theory of field

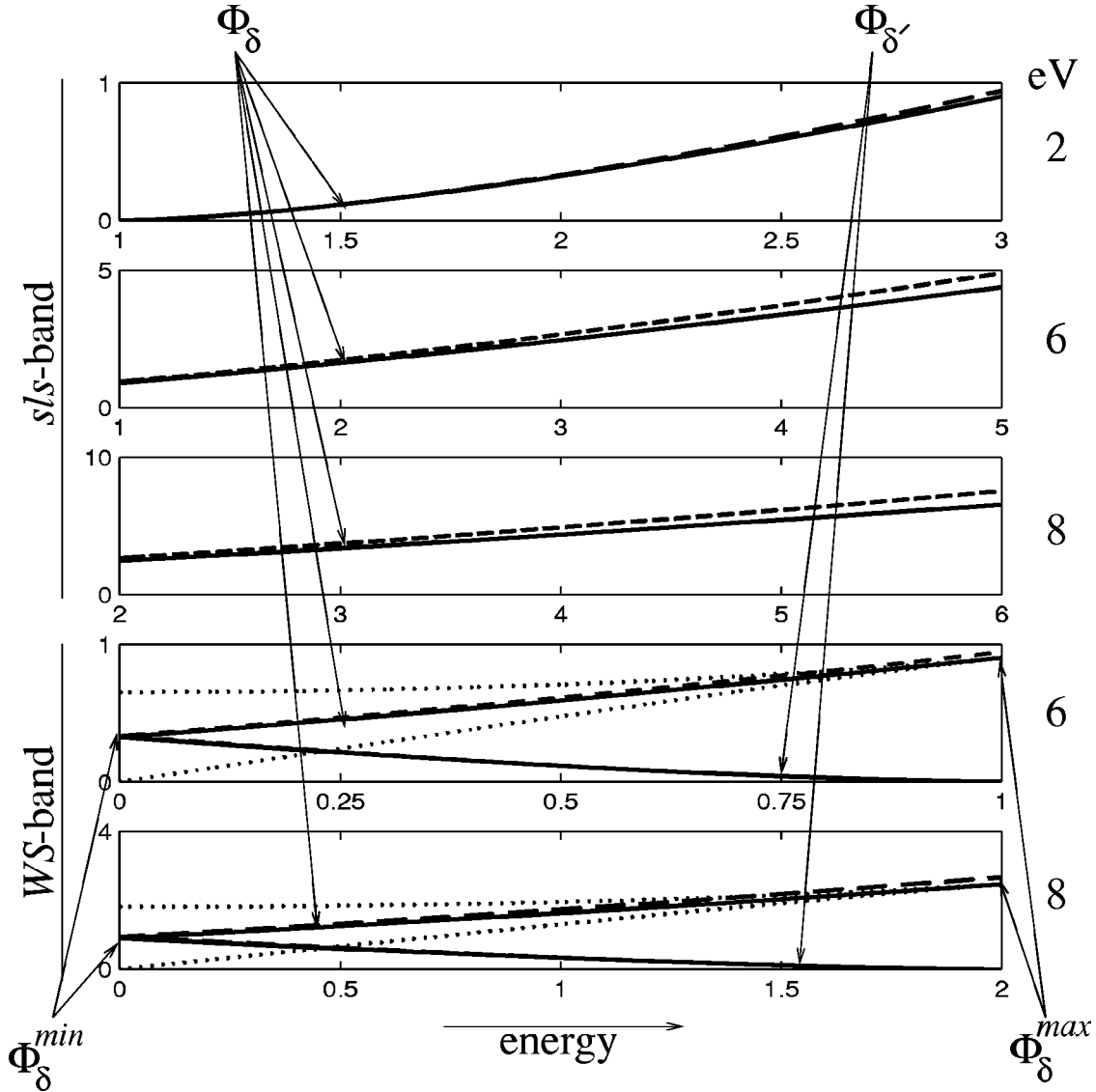


FIG. 6. Exact (solid lines) and approximate (dashed lines) dependencies  $\Phi_\delta(E)$  and  $\Phi_{\delta'}(E)$  as they are represented in the text. Function  $\Phi_\delta(E)$  is specified in Eqs. (11) (exact) and (14) (approximate);  $\Phi_{\delta'}(E)$  is represented in Eq. (16), and its approximate expression is given by Eq. (20). The three upper graphs correspond to the *sls* band. In the two lower graphs for the WS band, the rising and descending lines represent  $\Phi_\delta(E)$  and  $\Phi_{\delta'}(E)$ , respectively;  $3\Phi_\delta^{\min} = (eV/2)^{3/2}$ ,  $3\Phi_\delta^{\max} = (eV)^{3/2}$ . Functions  $\Phi^\pm = \Phi_\delta \pm \Phi_{\delta'}$  are plotted by dotted lines.

emission.<sup>51</sup> A qualitative difference in our result is that the exponent turns out to be dependent on  $eV$ . At high voltages the factor  $\exp[-4(E+eV)^{3/2}/(3\mathcal{E})]$  does not have any semiclassical analogy. In some more details, the interrelation between Eq. (13) and the WKB expression of the tunneling probability through a triangular barrier is discussed in Ref. 35.

*Effects of coupling on the transmission spectrum of the sls band.* The superlattice-to-lead connection is dependent on a number of factors. In Eq. (3) and subsequent equations, it is represented by a single parameter  $A$  which signifies the effective coupling.<sup>36</sup> It may vary by orders of magnitude in the relevant heterostructures. Therefore it is of interest to trace the dependence of the *sls*-band transmission spectrum on this parameter.

In the discussion about *es*-assisted tunneling, a common expectation has been mentioned that with the increase in

effective coupling, the resonance structure is smeared out. This is indeed true for the case of resonance tunneling as examined above. By contrast, as can be readily seen from Eq. (12), such an expectation is not justified for the *sls*-assisted tunneling. The peak positions and their sharpness are essentially determined by two cosine terms in the denominator of RHS in Eq. (12). In the absence of either of the two, the transmission spectrum would contain infinitely high resonances. This means that in both the extreme cases of weak coupling ( $A \approx 0$ ) and strong ( $A^2 \gg 1$ ) coupling, the *sls* transmission spectrum should have a well pronounced resonance structure. For the weak and strong couplings thus specified, the transmission peaks will be either at the *sls* energies  $E_n^{sls}$  or at zeros of  $\cos(2\Phi_\delta/\mathcal{E} - \pi/4)$ .

If the coupling is weak, the peak spacing repeats the level spacing within the *sls* band. In turn the latter is approximately equal to  $\mathcal{E}$ ,  $2\mathcal{E}$ , and ruled by the poles of the Airy

function within the corresponding parts of the *sls* band, see Fig. 1. These regularities can thus be observed in the *sls*-band transmission spectrum, as illustrated in Fig. 5(a) by open circles ( $\mathcal{E}$  spacing), filled circles ( $2\mathcal{E}$  spacing), and squares (Airy type spectrum).

For  $A^2 \gg 1$ , the position of the peaks in  $T(E)$  is determined by the zeros of the second summand of the denominator in Eq. (12) so that we have instead of Eq. (13)

$$T(E_p, \mathcal{E}) = \frac{4 \sinh \delta_p}{\sin \xi_p} \exp\left(-\frac{4}{\mathcal{E}} \Phi_{\delta_p}\right), \quad (15)$$

where the values of  $E_p$  are given by solutions to equation  $\cos(2\Phi_{\xi}/\mathcal{E} - \pi/4) = 0$ . These are shifted with respect to *sls* energies  $E_n^{sls}$ , and can be shown to obey the same regularities as those observed for the eigenvalues. The height of the peaks does not differ much in the cases of strong and weak coupling, as can be seen from the comparison of Eqs. (13) and (15). At the same time, if  $|A|$  is large, the wells between peaks are approximately  $A^2$  times deeper. Hence in the case of *sls*-assisted tunneling, the strong coupling with the leads makes the resonance structure of the transmission spectrum even more pronounced than that would be expected for the weak coupling. On the other hand, when the effective coupling is neither strong nor weak ( $|A| \approx 1$ ), Eq. (12) does not yield any pronounced structure. This unusual behavior of the *sls*-band transmission spectrum is illustrated by calculations of  $T(E)$  for different coupling constants  $|A| \ll 1$ ,  $|A| = 1$ , and  $|A| \gg 1$  in Fig. 5(b). One can see that with the increase in the interaction between the leads and tilted band, the transmission spectrum at first loses its resonance structure and then acquires it again with roughly interplaced peaks and wells, and deepened wells.

Summarizing the above analysis, the tunneling assisted by field-induced surface localized states, which appear as a result of the band tilting by the applied voltage, is characterized by a kind of unique (or at least not often observed) dependence of the transmission spectrum on the coupling to electron reservoirs involved. Some minimal voltage is required for the first *sls* to appear. This makes *sls*-assisted tunneling possible. A further increase in the applied potential results in the *sls*-band opening up to its maximal width  $E_{bw}$ . The increase of the *sls*-band width is accompanied by the

appearance of peaks in  $T(E)$  with the spacing governed by the following regularities. For  $eV < E_{bw}/2$ , the peak spacing is close to that of the Airy spectrum. For  $E_{bw}/2 < eV < E_{bw}$ , the Airy type peak spacing gradually changes to the double  $\mathcal{E}$  peak spacing characteristic for  $H_{nn'}$  eigenvalues in the middle of the maximum-width *sls* band. Finally for  $eV > E_{bw}$ , there is a third characteristic energy interval (close to the top of the WS band), where the peaks of the transmission probability are  $\mathcal{E}$  spaced. The latter spacing is commonly regarded as the WSL trademark.

## VI. TUNNELING ASSISTED BY WANNIER-STARK STATES

In the energy interval of bulk states (i.e., in the middle of the full spectrum, see Fig. 1), switching from low to high voltages results in an even more profound restructuring of the transmission spectrum. This can be expected since the *es* band, the states of which directly connect the source and drain leads, is replaced by the WS band, where the electronic states are localized between two mutually inverse triangular barriers. Tunneling through the *es* band was already discussed in Sec. IV. The treatment of WS-state assisted tunneling, which refers to the energy interval  $E < e\bar{V}/2 - \mathcal{E}$ , is similar to the analysis of the *sls*-band transmission spectrum.

In the present case however, the explicit expressions of the Green function matrix elements for large  $\mathcal{N}$  are different for the WSL energies  $E_n \approx n\mathcal{E}$  ( $\mathcal{N} = 2N + 1$ ) and for  $E \neq E_n$ . For the latter case we have

$$\left\{ \begin{array}{c} \mathcal{D}_{\mathcal{M}}(E, \mathcal{E}) \\ \mathcal{D}_{\mathcal{M}}(E, \mathcal{E}) G_{11}(E) \\ \mathcal{D}_{\mathcal{M}}(E, \mathcal{E}) G_{\mathcal{M}\mathcal{M}}(E) \end{array} \right\} \approx \frac{(-1)^N \mathcal{E} \sin(\pi E/\mathcal{E})}{\pi \sqrt{\sinh \delta \sinh \delta'}} \exp\left(\frac{2}{\mathcal{E}} \Phi^+\right) \times \left\{ \begin{array}{c} e^{\delta + \delta'} \\ e^{\delta'} \\ -e^{\delta} \end{array} \right\}, \quad (16)$$

where  $2 \cosh \delta' = eV/2 - E$ ,  $\Phi^+ = \Phi_{\delta} + \Phi_{\delta'}$ , and  $\Phi_{\delta'} = \delta' \cosh \delta' - \sinh \delta'$ . The use of Eq. (16) in Eq. (3) yields an explicit expression

$$T(E) \approx \frac{4A^2 \sinh \delta \sinh \delta'}{\sin^2(\pi E/\mathcal{E}) \{[\exp(\delta + \delta') - A^2]^2 + A^2(\exp \delta + \exp \delta')^2\}} \exp\left(-\frac{4}{\mathcal{E}} \Phi^+\right), \quad (17)$$

which provides an accurate description of the tunneling probability within the WS band, except the above indicated  $\mathcal{E}$  interval and energies close to values of  $n\mathcal{E}$ , see Fig. 7. For the WSL energies, instead of Eq. (17) we have

$$T(n\mathcal{E}, \mathcal{E}) \approx \frac{4 \sinh \delta_n \exp[-2(\delta_n - \delta'_n)]}{\sinh \delta'_n [1 + A^2 \exp(-2\delta_n)]} \exp\left(-\frac{4}{\mathcal{E}} \Phi_n^-\right), \quad (18)$$

where  $\Phi_n^- = \Phi_{\delta_n} - \Phi_{\delta'_n}$ ,  $2 \cosh \delta_n = eV/2 + n\mathcal{E}$ , and  $2 \cosh \delta'_n = eV/2 - n\mathcal{E}$ .

In the case of weak coupling, Eq. (18) has the same meaning for the WS band, as Eq. (13) has for the *sls* band. Under the replacement  $n\mathcal{E} \rightarrow E$  (hence  $\delta_n, \delta'_n, \Phi_n^- \rightarrow \delta, \delta', \Phi^- = \Phi_{\delta} - \Phi_{\delta'}$ , respectively) the function  $T(E)$  defined in Eq. (18) envelops the transmission spectrum over its local

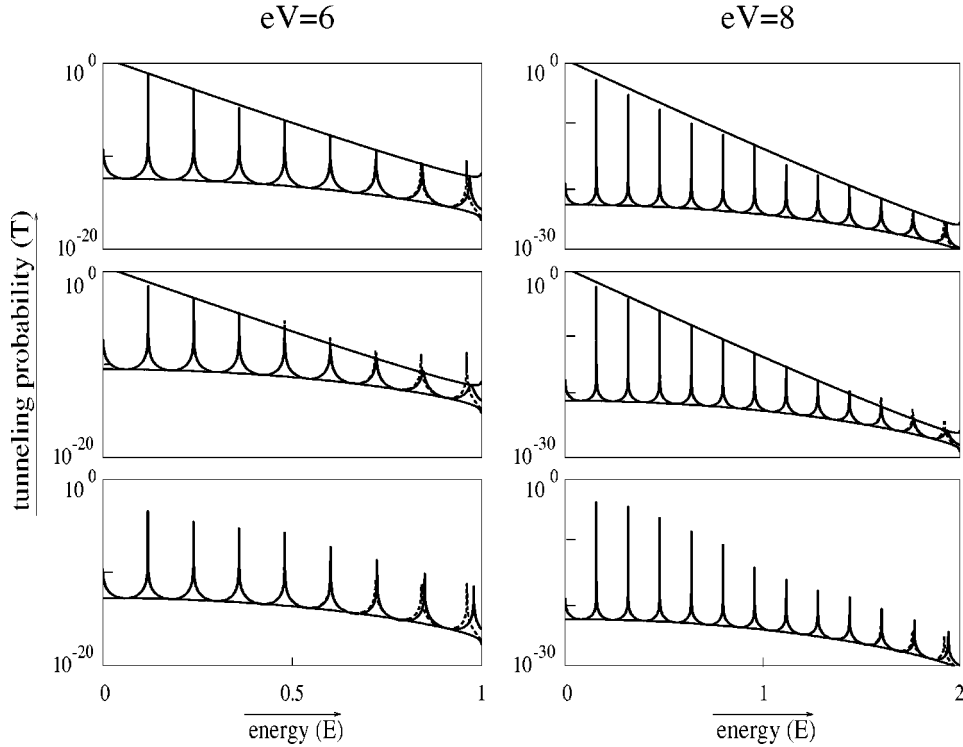


FIG. 7. Transmission spectrum of WS-states assisted tunneling through the lowest miniband of a 51-well superlattice. The solid and dashed oscillating lines represent exact and approximate expressions of  $T(E)$  given in Eqs. (3) and (18), respectively. The maxima envelope corresponds to Eq. (18) with  $n\mathcal{E}$  replaced by  $E$ , and minima envelope corresponds to Eq. (19). In upper part  $|A|=0.1$ ; in the middle,  $|A|=1$ ; and for two lower graphs,  $|A|=100$ .

maxima. The envelope is reproduced equally well by Eq. (10a) with the replacement of the trigonometric functions which appear in expression (10a), by their hyperbolic counterparts.

By analogy the expression of the transmission coefficient, that follows from Eq. (17) at the energies  $E_n = (n + 1/2)\mathcal{E}$  (for odd  $\mathcal{N}$ ), may be called the minima envelope. Its expression is given by

$$T(E) \approx \frac{4A^2 \sinh \delta \sinh \delta'}{[\exp(\delta + \delta') - A^2]^2 + A^2(\exp \delta + \exp \delta')^2} \times \exp\left(-\frac{4}{\mathcal{E}}\Phi^+\right). \quad (19)$$

The maxima- and minima-enveloping functions shown in Fig. 7 exhibit a striking difference in their dependence on energy. The reason for this can be clarified by using approximation (14) and its analog for  $\Phi_{\delta'}$

$$3\Phi_{\delta'} \approx \overline{(eV/2 - E)^{3/2}}, \quad (20)$$

the accuracy of which is illustrated in Fig. 6. The exponents of the enveloping functions are thus defined simply as a difference  $(4\Phi^-/\mathcal{E})$  and a sum  $(4\Phi^+/\mathcal{E})$  of two FN-type exponents  $4(eV/2 + E)^{3/2}/(3\mathcal{E})$  and  $4(eV/2 - E)^{3/2}/(3\mathcal{E})$ . It is noticeable that Eqs. (14) and (20) meet the requirements  $\Phi^- = 0$ ,  $\Phi^+ = 2\Phi_{\delta'}^{\min} = e\overline{V^{3/2}}/(3\sqrt{2})$  at the middle of the WS band  $E=0$ , and  $\Phi^+ = \Phi^- = \Phi_{\delta'}^{\max} = e\overline{V^{3/2}}/3$  at the top of the WS band  $E=eV/2$ . These estimates make it easily quantifiable that there is a huge difference between the maxima and minima envelopes in the middle of the WS band.

An extremely sharp resonance structure, exhibited by the transmission spectrum of the WS-state assisted tunneling, has the same nature as the well-known phenomenon of resonance tunneling through a barrier-well-barrier structure. In the given case, the barriers are of a triangular shape. The structure is only totally symmetric (and the transmission coefficient is equal or close to unity for odd and even  $\mathcal{N}$ , respectively) at the middle of the spectrum  $E=0$ . The increase or decrease in energy strongly suppresses the local maxima of electron transmission because of the increasing system asymmetry. In contrast, because the total length of the two barriers is independent of energy, the minima envelope of  $T(E)$  does not depend on energy so strongly.

As can be concluded from Eqs. (18) and (19) and is exemplified in Fig. 7, the sharpness of the resonance structure in the case of electron transmission through the WS band is largely insensitive to the coupling strength unlike the *s/s*-assisted tunneling. Hence tunneling through the midpart of a tilted band may serve as a nearly ideal energy filter. The anomalous sharpness and exponential decrease of the equidistant peaks can also be regarded as a distinctive signature of Bloch oscillations in tunneling through the tilted band and related phenomena such as Zener tunneling through a third band<sup>47</sup> and Franz-Keldysh oscillations.<sup>31</sup>

## VII. TUNNELING THROUGH THE TRAPEZOID BARRIER

In this section we briefly consider the case of tunneling indicated in Fig. 3 by the TB arrow. The energy is thus supposed to be outside the tilted band  $E > (E_{\text{bw}} + eV)/2$ . For large  $\mathcal{N}$  and small  $\mathcal{E}$ , the use of approximate expressions similar to Eq. (16) in the transmission probability (3) gives

$$T(E) = \frac{16A^2 \sinh \alpha \sinh \delta \exp[-2(\alpha + \delta)]}{1 + A^2[\exp(-2\alpha) + \exp(-2\delta)] + A^4 \exp[-2(\alpha + \delta)]} \exp\left[-\frac{4}{\mathcal{E}}(\Phi_\delta - \Phi_\alpha)\right], \quad (21)$$

where  $2 \cosh \alpha = E - eV/2$ . The definition of  $\alpha$  differs from that of  $\delta'$  only by an interreplacement  $E \leftrightarrow eV/2$ , see Eq. (16).

Under the restrictions indicated above, the energy and field dependence described by Eq. (21) (solid lines in Fig. 8) is in excellent agreement with the model exact Eq. (3). A divergence is only appreciable for the energies which are close to the *sls* band. For this latter region Eq. (21) predicts a somewhat different probability of tunneling if compared with the exact values of  $T(E)$  (the difference is not seen in Fig. 8).

Equation (21) and particularly, the exponential factor  $\exp[-4(\Phi_\delta - \Phi_\alpha)/\mathcal{E}]$  looks very much distinct from the usual WKB expression of the tunneling probability through a trapezoid barrier. Nevertheless the equivalence of Eq. (21) and WKB result for  $eV \ll E_{bw}$  can be proved by passing to the continuous limit. This can be done in the same way as the Fowler-Nordheim-type exponential factor has been derived from Eq. (13).<sup>35</sup> Skipping rather tedious calculations, here we only present the final result for the WKB equivalent of Eq. (21) (dashed line in Fig. 8)

$$T_{\text{WKB}}(E) = \frac{16A^2 \sinh^2 \delta \exp(-2\delta)}{[1 + A^2 \exp(-2\delta)]^2} \times \exp\left[-2\delta \mathcal{N} \left(1 - \frac{eV}{4\delta^2}\right)\right]. \quad (22)$$

On the other hand, in the zero-field limit, Eq. (21) transforms into

$$T^{(0)}(E) = \frac{16A^2 \sinh^2 \delta^{(0)} \exp(-2\delta^{(0)})}{[1 + A^2 \exp(-2\delta^{(0)})]^2} \exp(-2\delta^{(0)} \mathcal{N}), \quad (23)$$

where  $2 \cosh \delta^{(0)} = E$ . It is seen that without the second term in the exponent, Eq. (22) as a function of  $\delta$  coincides with the zero-field expression (23) as a function of  $\delta^{(0)}$ ;  $\delta$  and  $\delta^{(0)}$  signify the imaginary electron wave vector within the barrier.

This result proves the identity of  $T_{\text{WKB}}(E)$  with Eq. (21) in a zero-field limit. Moreover up to the values of  $eV$  comparable with  $E_{bw}$ , the WKB expression (22) describes tunneling through a trapezoid barrier reasonably well, see Fig. 8, but it fails in the case of high voltages. It is worth recalling that we are discussing trapezoid barriers capped by a tilted band, and not by an unbounded free electron spectrum.

So Eqs. (21), (12), and (17) give an accurate explicit description of electron tunneling specified in Fig. 3 by TB, FN, and WS arrows, respectively. Equation (17) corresponds to a purely quantum case of WS-states assisted tunneling and therefore it does not have a semiclassical analog, as do Eqs. (12) and (21).

## VIII. CONCLUSION

The transmission probability, describing electron ballistic transport between two leads connected electronically via a single tilted band, is presented as an explicit function of the electron energy, the electric field parameter, the thickness of the contact (given by a superlattice, dielectric layer, or relevant item) and the parameter of lead effective coupling to the contacting region. The derived expressions bring to light all the characteristic dependencies of the tunnel event, facilitating the understanding of every point that one would like to know about this particular model of electric field effects on tunneling. A number of conclusions are made throughout the discussion and their manifold physical and experimental implications are illustrated in various ways. No doubt all of them were to some extent present in numerous related studies but had never been elucidated with the present degree of explicitness and completeness covering all the typical situations consistent with the model.

An experimental verification of our results requires a

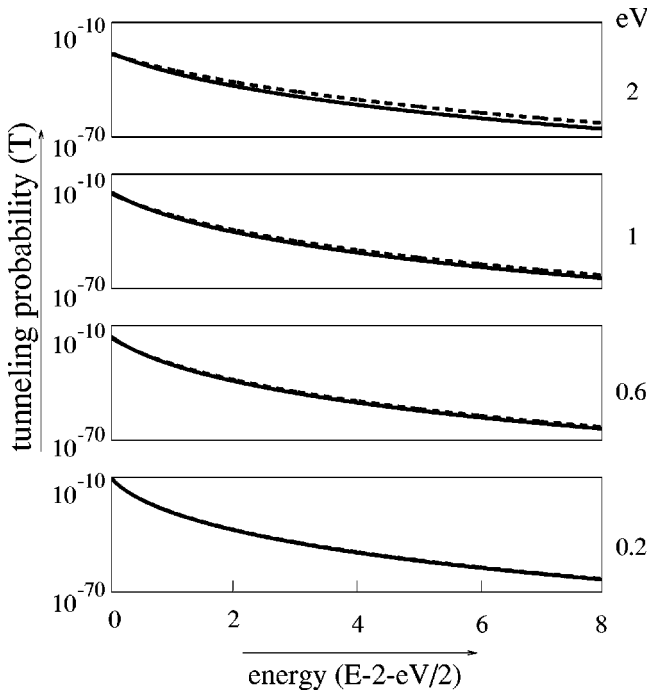


FIG. 8. Tunneling probability above (or below) the tilted band, calculated from Eqs. (21) and (22) for different voltages (as indicated), is represented by solid and dashed lines, respectively. In calculations,  $\mathcal{N} = 51$ ,  $|A| = 0.1$ .

technique which allows one to measure the energy dependence of the electron transmission coefficient directly and at different applied voltages. This is a challenging experimental problem which can be solved by means of ballistic-electron-emission microscopy<sup>52</sup> or other specially designed techniques. For more traditional and less informative methods of the tunneling-current spectroscopy, the observation of predicted effects seems to be more problematic. The current response to a change in the applied voltage is contributed to by a combination of all electron states within the corresponding energy interval near the Fermi energy. The summation of the contributions, that is the integration of the transmission coefficient preserves some structure of  $I$ -on- $V$  dependence which is incomparably less pronounced than that of the transmission spectrum. However, the predicted exponential dependencies remain easily recognizable and can be used for the interpretation of the current spectroscopy experiments. The obtained explicit forms of the transmission coefficient make it easy to predict what kind of the  $I$ - $V$  relation should be expected. At the same time the particular form of the  $I(V)$

curve is also strongly dependent on the zero-field position of the Fermi energies in the contacting leads and the portion of the total electrostatic potential which drops linearly along the tunneling region. Therefore modeling of  $I$ - $V$  relations only makes sense in the context of specified samples and experimental conditions. This goes beyond the scope of the present analysis.

Further generalization of the presented results, to cover the two-band processes such as Zener tunneling and Franz-Keldysh effect, looks highly desirable. In this respect, the understanding and methodology developed are helpful but not sufficient to attain the goal. Work in this direction is currently in progress.

### ACKNOWLEDGMENTS

This work was supported by the Swedish Research Council. Partial support from INTAS under Grant No. 99-864 is also gratefully acknowledged.

\*Address for communication: Division of Physics, Luleå University of Technology, SE-971 87 Luleå, Sweden. Electronic address: alex@mt.luth.se

- <sup>1</sup>G. H. Wannier, Phys. Rev. **117**, 432 (1960); Rev. Mod. Phys. **34**, 645 (1962).
- <sup>2</sup>E. E. Mendez and G. Bastard, Phys. Today **46**, 34 (1993).
- <sup>3</sup>F. Rossi, Semicond. Sci. Technol. **13**, 147 (1998).
- <sup>4</sup>K. Leo, Semicond. Sci. Technol. **13**, 249 (1998).
- <sup>5</sup>D. H. Dunlap and M. V. Kenkre, Phys. Rev. B **34**, 3625 (1986).
- <sup>6</sup>M. Holthou, Phys. Rev. Lett. **69**, 351 (1992).
- <sup>7</sup>M. Holthou, Z. Phys. B **89**, 251 (1992).
- <sup>8</sup>M. Holthou and D. Hone, Phys. Rev. B **69**, 6499 (1993).
- <sup>9</sup>S. R. Wilkinson, C. F. Bharucha, K. W. Madison, Q. Niu, and M. G. Raizen, Phys. Rev. Lett. **76**, 4512 (1996).
- <sup>10</sup>Q. Niu, X.-G. Zhao, G. A. Georgakis, and M. G. Raizen, Phys. Rev. Lett. **76**, 4504 (1996).
- <sup>11</sup>M. G. Raizen, C. Salomon, and Q. Niu, Phys. Today **50**, 30 (1997).
- <sup>12</sup>K. W. Madison, M. C. Fischer, R. B. Diener, Q. Niu, and M. G. Raizen, Phys. Rev. Lett. **81**, 5093 (1998).
- <sup>13</sup>K. W. Madison, M. C. Fischer, and M. G. Raizen, Phys. Rev. A **60**, R1767 (1999).
- <sup>14</sup>M. Glück, M. Hankel, A. R. Kolovsky, and H. J. Korsch, Phys. Rev. A **61**, 061 402(R) (2000).
- <sup>15</sup>J. Zak, Phys. Rev. Lett. **20**, 1477 (1968).
- <sup>16</sup>K. Hacker and G. Obermair, Z. Phys. **234**, 1 (1970).
- <sup>17</sup>G. C. Stey and G. Gusman, J. Phys. C **6**, 650 (1973).
- <sup>18</sup>M. Saitoh, J. Phys. C **6**, 3255 (1973).
- <sup>19</sup>H. Fukuyama, R. A. Bari, and H. C. Fogedby, Phys. Rev. B **8**, 5579 (1973).
- <sup>20</sup>A. I. Onipko, L. I. Malysheva, and Yu. A. Klimenko, Physica B **225**, 125 (1996).
- <sup>21</sup>S. G. Davison, R. A. English, A. L. Mišković, F. O. Goodman, A. T. Amost, and B. L. Burrows, J. Phys.: Condens. Matter **9**, 6371 (1997).
- <sup>22</sup>L. I. Malysheva, Ukr. Fiz. Zh. **45**, 1475 (2000).
- <sup>23</sup>V. M. Yakovenko and H.-S. Goan, Phys. Rev. B **58**, 8002 (1998).
- <sup>24</sup>A. Onipko and L. Malysheva, Solid State Commun. **118**, 63 (2001); Phys. Rev. B **63**, 235 410 (2001).
- <sup>25</sup>C. Zener, Proc. R. Soc. London **145**, 523 (1934).
- <sup>26</sup>W. Franz, Z. Naturforsch. Teil A **13**, 484 (1958); L. V. Keldysh, Zh. Éksp. Teor. Fiz. **34**, 1138 (1958) [Sov. Phys. JETP **34**(7), 788 (1958)].
- <sup>27</sup>K. B. McAfee, E. J. Ryder, W. Shockley, and M. Sparks, Phys. Rev. **83**, 650 (1951).
- <sup>28</sup>L. V. Keldysh, Zh. Éksp. Teor. Fiz. **33**, 994 (1957) [Sov. Phys. JETP **6**, 763 (1958)].
- <sup>29</sup>E. O. Kane, J. Phys. Chem. Solids **12**, 181 (1959).
- <sup>30</sup>P. N. Argyres, Phys. Rev. **126**, 1386 (1962); **134**, A998 (1964).
- <sup>31</sup>J. Callaway, Phys. Rev. **130**, 549 (1963); **134**, A998 (1964).
- <sup>32</sup>D. E. Aspnes, Phys. Rev. **147**, 554 (1966).
- <sup>33</sup>D. E. Aspnes and N. Bottka, in *Semiconductors and Semimetals*, edited by R. K. Willardson and A. C. Beer (Academic Press, New York, 1972), Vol. 9.
- <sup>34</sup>This can be seen already from the fact that the exponential factor turns out to be dependent on the characteristics of the zero-field bands. However, as is shown in this work, such a description is appropriate only near the band edges and strictly speaking only in the case of low voltages.
- <sup>35</sup>A. Onipko and L. Malysheva (unpublished).
- <sup>36</sup>A. Onipko, Yu. Klymenko, and L. Malysheva, Phys. Rev. B **62**, 10 480 (2000).
- <sup>37</sup>R. Landauer, IBM J. Res. Dev. **1**, 323 (1957); Philos. Mag. **21**, 683 (1970).
- <sup>38</sup>M. Büttiker, Y. Imry, R. Landauer, and S. Pinhas, Phys. Rev. B **31**, 6207 (1985).
- <sup>39</sup>A. D. Stone and A. Szafer, IBM J. Res. Dev. **32**, 384 (1988).
- <sup>40</sup>C. B. Duke, in *Solid State Physics*, edited by F. Seitz and D. Turnbull (Academic Press, New York, 1969), Suppl. 10.
- <sup>41</sup>S. Datta, *Electronic Transport in Mesoscopic Systems* (Cambridge University Press, Cambridge, 1995).
- <sup>42</sup>C. Caroli, R. Combescot, P. Nozières, and D. Saint-James, J. Phys. C **4**, 916 (1971).

- <sup>43</sup>V. Mujica, M. Kemp, and M. A. Ratner, *J. Chem. Phys.* **101**, 6849 (1994); **101**, 6856 (1994).
- <sup>44</sup>A. Onipko, *Phys. Rev. B* **59**, 9995 (1999).
- <sup>45</sup>A. I. Onipko, K.-F. Berggren, Yu. O. Klymenko, L. I. Malysheva, J. J. W. M. Rosink, L. J. Geerligs, E. van der Drift, and S. Radelaar, *Phys. Rev. B* **61**, 11 118 (2000).
- <sup>46</sup>J. G. Simmons, *J. Appl. Phys.* **34**, 1793 (1963).
- <sup>47</sup>A. Di Carlo, P. Vogl, and W. Pötz, *Phys. Rev. B* **50**, 8358 (1994).
- <sup>48</sup>N. Linder, K. H. Schmidt, W. Geisselbrecht, G. H. Döhler, H. T. Grahn, K. Ploog, and H. Schneider, *Phys. Rev. B* **52**, 17 352 (1995).
- <sup>49</sup>B. Ricco and M. Azbel, *Phys. Rev. B* **29**, 1970 (1984).
- <sup>50</sup>M. Abramowitz and I.A. Stegun, *Handbook of Mathematical Functions* (Dover, New York, 1965).
- <sup>51</sup>R. H. Fowler and L. Nordheim, *Proc. R. Soc. London, Ser. A* **119**, 173 (1928).
- <sup>52</sup>D. L. Smith and S. M. Kogan, *Phys. Rev. B* **54**, 10 354 (1996), and references therein.